*Int. J. Electrochem. Sci.*, 15 **(2020)** 2499 – 2510, doi: 10.20964/2020.03.76

International Journal of
ELECTROCHEMICAL
SCIENCE
www.electrochemsci.org

# 1-Phenyl-1H-tetrazole-5-thiol as corrosion inhibitor for Q235 steel in 1 M HCl medium: Combined experimental and theoretical researches

*Jia Liu*[1,*], *Yang Zhou*[2*], *Chengyu Zhou*[1], *Hao Lu*[1,*]

[1] School of Chemistry and Chemical Engineering, Chongqing University of Science and Technology, Chongqing 401331, P.R. China
[2] Analytical and Testing Center, Chongqing University, Chongqing 400044, P.R.China
[*]E-mail: Liujia901@cqust.edu.cn (J. Liu), zhoucy0130@cqust.edu.cn (Y. Zhou), 2019047@cqust.edu.cn (H. Lu)

*Received:* 17 November 2019 / *Accepted:* 13 January 2020 / *Published:* 10 February 2020

1- Phenyl-1H-tetrazole-5-thiol (PTZ) as a novel corrosion inhibitor for Q235 steel in 1 M HCl solution was researched via experimental and theoretical ways. In this work, we used a variety of research methods including electrochemical impedance spectroscopy (EIS) measurement, potentiodynamic polarization (PDP) curves, scanning electron microscopy (SEM), quantum chemical calculations and molecular dynamics simulation (MDS). The data of PDP curves manifest that PTZ is a mixed type corrosion inhibitor. The inhibition efficiency is 97.1 % when the PTZ concentration is 5 mM at 298 K. The data of EIS showed that the charge transfer resistance became significantly larger as the concentration of PTZ increased. This indicates that the protective film formed by PTZ on the surface of Q235 steel can effectively inhibit the corrosion of Q235 steel. SEM analysis test results strongly support the electrification data. Besides, the PTZ adsorption on the surface of Q235 is obey Langmuir adsorption. Theoretical calculation experiments further reveal that PTZ can show excellent corrosion inhibition performance.

**Keywords:** 1-Phenyl-1H-tetrazole-5-thiol; Q235 steel; HCl; corrosion inhibitor; EIS; SEM; Langmuir adsorption

## 1. INTRODUCTION

With the economic development and social progress, the use of various metal products is increasing [1]. Industrialization has provided a broad stage for metal materials, and has also accelerated the corrosion of metals, making metal corrosion and protection work more important [2]. Each year, the

global metal loss caused by corrosion accounts for about 30% of the total metal production [3]. Therefore, it is necessary to do a good job of metal corrosion and protection.

Metal corrosion is a phenomenon in which materials deteriorated and destroyed by the chemical or electrochemical effects of environmental media [4]. This is a spontaneous process. The metal is in contact with the electrolyte solution in the environment, and a potential difference is formed between impurities in the metal or different kinds of metals, which constitutes the corrosion of the galvanic cell and causes the metal corrosion. This phenomenon is called electrochemical corrosion. The corrosion process can be divided into two independent and simultaneous anode (oxidation) and cathode (reduction) processes. The variety of metal materials and the complexity of the corrosion environment determine the variety of metal corrosion protection methods.

Among the many methods of metal corrosion protection, corrosion inhibitors have been widely used due to their low usage, simple operation, and mature technology [5]. Corrosion inhibitors can be divided into organic corrosion inhibitors and inorganic corrosion inhibitors. Due to the large amount of inorganic corrosion inhibitor, it will cause a great deal of pollution to the environment. Therefore, the use of inorganic corrosion inhibitors has been greatly restricted. Organic corrosion inhibitor molecules usually contain heteroatoms (P, S, N, and O) and some polar functional groups [6-12]. These heteroatoms contain unbonded lone electron pairs that can form coordination bonds with the empty orbits of the metal. Thus forming chemisorption on the metal surface. In addition, the inhibitor molecules and metal surfaces can be physically adsorbed by electrostatic interaction. Therefore, most of the inhibitor molecules can interact on the surface of the metal through physical and chemical adsorption.

In this paper, we studied the anti-corrosion performance of PTZ for Q235 steel in 1 mol/L hydrochloric acid medium. The molecular formula of PTZ is listed in Figure 1. We can find that PTZ molecule contain one sulfur and four nitrogen atoms. Therefore, we can reasonably judge its potential as an effective corrosion inhibitor for Q235 steel in 1 mol/L hydrochloric acid medium. Through electrochemical, surface morphology research, and theoretical calculations from the experimental and theoretical perspectives to explore the anti-corrosion performance of PTZ.

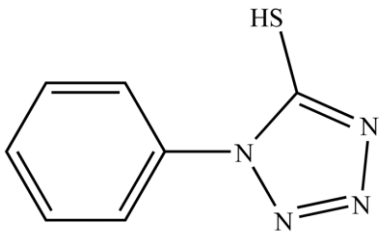


**Figure 1.** Molecular structure of PTZ.

## 2. EXPERIMENTAL

### *2.1 Materials preparation*

The PTZ purchased from Adamas Reagents. Its purity is 99.5%. The chemical composition of Q235 steel is as follow: Mn (0.14 %), Si (0.19 %), P (0.04 %), C (0.17 %), S (0.04 %) and Fe (99.44 %).

Q235 steel was cut into 1×1×1 $cm^3$ pieces for making working electrode. Q235 steel was sealed with epoxy resin leaving only a 1×1 $cm^2$ area. The working electrode was sanded on 400, 800, 1200, and 2000 mesh sandpapers before electrochemical testing. After polishing, the electrode was ultrasonically irradiated with ultrapure water and absolute ethanol. Finally, in the cold air state, the electrode is dried.

The 1 mol/L hydrochloric acid was prepared using high purity hydrochloric acid and ultrapure water. The 1 mol/L hydrochloric acid without PTZ as a blank solution for comparison. PTZ was sequentially prepared into 0.04 mM, 0.2 mM, 1 mM and 5 mM test solution.

### *2.2 Surface topography test*

Q235 steel was cut into 0.5×0.5×0.5 $cm^3$ samples for scanning electron microscopy measurement (JEOL-JSM-7800F). Carefully sand the Q235 steel samples on 400 to 7000 mesh sandpapers. Then, the polished Q235 steel samples were cleaned with ultrapure $H_2O$ and absolute ethanol. Finally, the Q235 steel samples were immersed in 1 mol/L hydrochloric acid without and with 5 mM PTZ for 6 hours at 298 K. The soaking time is over, the Q235 steel sample is rinsed with ultrapure water.

### *2.3 Electrochemical tests*

In this work, the electrochemical experiments were tested on the Chi760e electrochemical workstation (Shanghai Chenhua Co., Ltd.) with classical three-electrode cell. The test temperature of all experiments is 298 K via a thermostatic water bath to keep the temperature constant. In this three-electrode cell, Q235 steel is the working electrode with 1×1 $cm^2$ area. Saturated calomel electrode (SCE) is a reference electrode connect a vitreous Luggin capillary to reduce solution impedance. Platinum sheet is a reference electrode. Before conducting the electrochemical tests, firstly, the Q235 steel electrode was dipped in the tested solution for 1200 s to obtain a stabilized state. Record the potential of open circuit value ($E_{OCP}$) after stabilization. EIS was performed with the stable $E_{OCP}$ value. The frequency range was 100000 Hz to 10 mH Hz, and sinusoidal excitation signal wave was 5 mV. Finally, the PDP curves were tested. The polarization range was $E_{OCP} \pm 250$ mV, and the scanning rate was 0.01 mV/s.

### *2.4 Theoretical calculation*

The quantum chemical calculations and molecular dynamics simulation of PTZ was performed using Material Studio software. The calculated parameter settings were as followings: the structural optimization as the task of calculation. Quality was fine. Energy was $4\times10^{-5}$ Ha. Max.force was 0.05 Ha/Å. Basis Set and Basis file were DNP and 4.4, respectively. The COMPASS was selected as the Forcefield. The adsorption configuration of PTZ and 500 $H_2O$ molecules on the Fe (110) surface was calculated via the forcite module. The parameters were set as following: Dynamics as the calculated task. Qualit was medium. Ensemble was NVT. Time step was 1fs, and Total simulation time was 1000 ps.

## 3. RESULTS AND DISCUSSION

### *3.1. Electrochemical impedance spectroscopy*

Figure 2 shows Niqust plot and Bode plot at different PTZ concentrations for Q235 steel in 1 mol/L hydrochloric acid at 298 K. As shown in Figure 2(a), as the concentration of PTZ increases, the radius of the capacitive loop increases significantly. This indicates that the charge transfer resistance is increased due to the adsorption of PTZ, which has a significant inhibitory effect on the corrosion of Q235 steel. The shapes of Niqust plot have not changed significantly, indicating that the adsorption of PTZ on the surface of Q235 steel has little change in its reaction mechanism.

As shown in Figure 2b, in the low frequency region, the capacitive reactance modulus is significantly increased by an order of magnitude. In addition, in the intermediate frequency region, the slope of the impedance modulus can be found to be close to 1. It indicates that PTZ has a capacitance property in Q235 steel. In addition, it can be seen that only one peak appears in the phase angle, indicating that PTZ only produces a time constant when adsorbed on the surface of Q235 steel. In addition, it can be found that as the concentration of PTZ increases, the phase angle map becomes significantly wider. Therefore, these test results show that PTZ molecules form a dense molecule film on the Q235 steel surface, which effectively inhibits the corrosion of Q235 steel in acid medium.

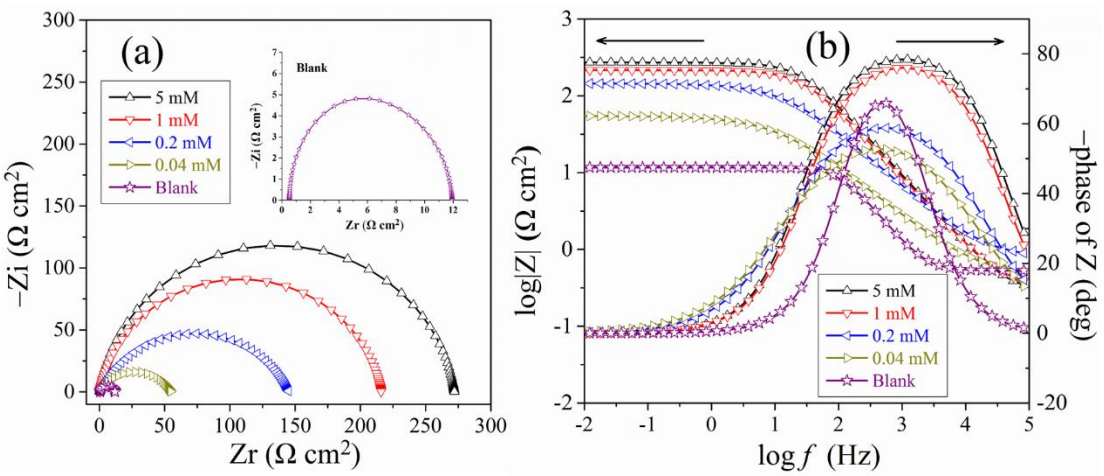


**Figure 2.** The plots of the Nyquist and Bode for Q235 steel in1 mol/L hydrochloric acid with PTZ without different concentrations of PTZ at 298 K.

In order to understand the electrochemical impedance spectroscopy in depth, we used the equivalent circuit diagram (Figure 3) to fit the electrochemical impedance spectroscopy data. Where $R_s$ stands for the solution resistance, $R_{ct}$ is the charge transfer resistance, and *CPE* stands for the constant phase angle element. The fitted experimental data is listed in Table 1. The formula for $\eta$ is obtained by the following formula [13-18]:

$$\eta(\%) = \frac{R_{ct} - R_{ct,0}}{R_{ct}} \times 100 \qquad (1)$$

where $R_{ct,0}$ and $R_{ct}$ stand for charge transfer resistance in the absence and presence PTZ, respectively. It can be found that the charge transfer resistance ($R_{ct}$) in the blank solution is 11.2 Ω cm$^2$ in the Table 1. When the PTZ concentration is 5 mM, the value of the charge transfer resistance sharply increases to 271.8 Ω cm$^2$. The corrosion inhibition efficiency is 95.9%. This shows that PTZ exhibits excellent corrosion inhibition performance. In Table 1, the electric double layer capacitance ($C_{dl}$) can be calculated by the following formulas [19, 20]:

$$Z_{CPE} = \frac{1}{Y_0(j\omega)^n} \quad (2)$$

$$C = Y_0(\omega)^{n-1} = Y_0(2\pi f_{Z_{im-Max}})^{n-1} \quad (3)$$

As shown in Table 1, the values of $C_{dl}$ decrease significantly as the concentration of PTZ increases, because PTZ replaces the water molecules on the surface of Q235 steel. it can be found that the $C_{dl}$ values in the blank solution is 150.9 μF cm$^{-2}$. As the concentration of PTZ increases, the $C_{dl}$ values show a downward trend. When the PTZ concentration is 5 mM, the value of $C_{dl}$ drops sharply to 13.2 μF cm$^{-2}$. Which is explained by the following formula [21]:

$$C_{dl} = \frac{\varepsilon^0 \varepsilon}{d} S \quad (4)$$

According to formula 4, it is found that the more the value of $C_{dl}$ decreases, indicating that the more water molecules were replaces the surface of Q235 steel, the denser the protective film is formed. In addition, it is worth mentioning that the value of the deviation index n is significantly close to 1. As the concentration of PTZ increases, this indicates that PTZ forms a dense protective film on the surface of Q235 steel.

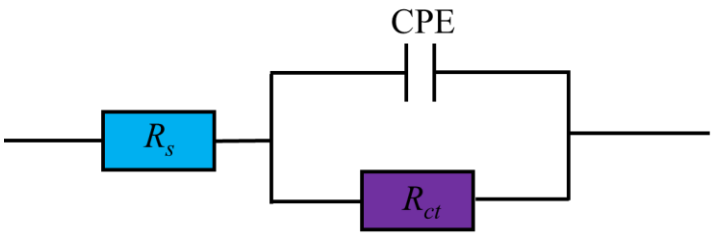


**Figure 3.** Equivalent circuit diagram for fitting impedance spectrum data.

**Table 1.** Impedance spectrum data

| C (mM) | $R_s$ (Ω cm$^2$) | $Y_0 \times 10^{-6}$ (S s$^n$ cm$^{-2}$) | $n$ | $C_{dl}$ (μF cm$^{-2}$) | $R_{ct}$ (Ω cm$^2$) | $\eta$ (%) |
|---|---|---|---|---|---|---|
| Blank | 0.52 | 134.2 | 0.81 | 150.9 | 11.2 | - |
| **PTZ** | | | | | | |
| 0.04 | 0.42 | 97.0 | 0.83 | 42.1 | 54.4 | 79.4 |
| 0.2 | 0.75 | 24.3 | 0.85 | 44.5 | 144.3 | 92.2 |
| 1 | 0.33 | 4.6 | 0.89 | 24.1 | 215.6 | 94.8 |
| 5 | 0.27 | 3.6 | 0.92 | 13.2 | 271.8 | 95.9 |

*3.2. Open circuit potential and Polarization curves analysis*

Figure 4 (a) and (b) shows the open circuit potential curves and potentiodynamic polarization curves at different concentrations of PTZ at 298 K, respectively. As shown in Figure 4 (a), after immersing Q235 steel in a 1 M hydrochloric acid solution for 1200 s, the open-circuit potential tends to stabilize. This indicates that the surface of Q235 steel has nearly reached an equilibrium state.

It can be found that the corrosion current density decreases significantly with the increase of PTZ concentration. This indicates that PTZ can effectively inhibit the corrosion of Q235 steel in 1 M HCl solution. All of the cathodic polarization curves in Figure 4 showed a parallel trend, indicating that the adsorption of PTZ on the surface of the Q235 steel did not change the reaction mechanism of the cathode. The slope of the anodic branch curves is clearly changed, indicating that the mechanism of the anodic reaction has changed. That is to say, the adsorption of PTZ on the surface of Q235 steel can effectively inhibit the dissolution of $Fe^{2+}$.

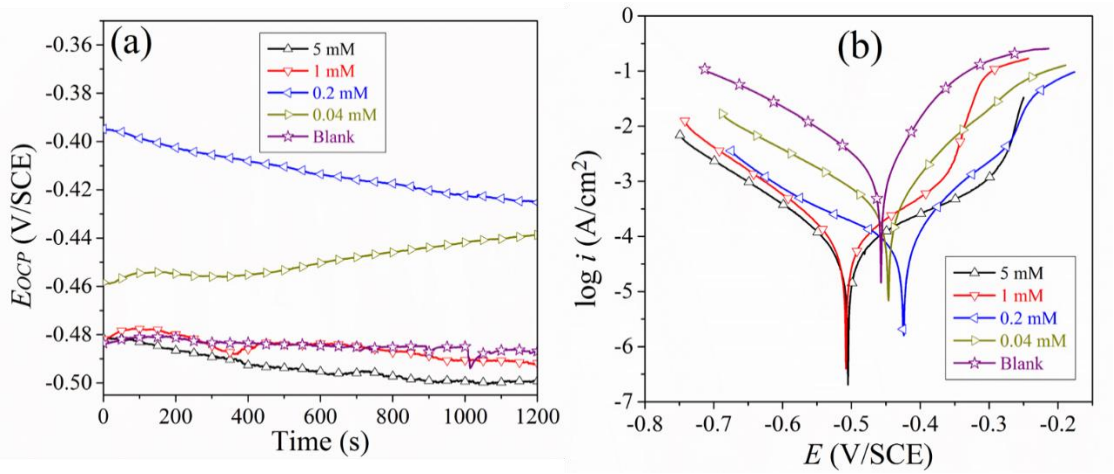


**Figure 4.** (a) and (b) shows the open circuit potential curves and potentiodynamic polarization curves at different concentrations of PTZ at 298 K, respectively.

The Tafel extrapolation method was used to obtain the corrosion current density, the corrosion potential, and the slope of the anode and cathode. The obtained data are listed in Table 2.The corrosion current density is obtained by the following formula [22-28]:

$$\eta(\%) = \frac{i_{corr,0} - i_{corr}}{i_{corr,0}} \times 100 \qquad (5)$$

where $i_{corr,\,0}$ and $i_{corr}$ stand for corrosion current density without and with PTZ, respectively. In the blank solution without PTZ added, the value of the corrosion potential was −0.457 V, and the corrosion potential gradually decreased as the concentration of PTZ increased. While the magnitude of the change is significantly less than 85 mV. it indicates that PTZ is a mixed type of corrosion inhibitor for Q235 steel in 1 M HCl medium [29].

**Table 2.** The polarization curves data of Q235 steel in 1 M HCl with and without different concentrations of PTZ at 298 K.

| *C* (mM) | $E_{corr}$(V/SCE) | $i_{corr}$(μA cm$^{-2}$) | $\beta_c$(mV dec$^{-1}$) | $\beta_a$(mV dec$^{-1}$) | $\eta$ (%) |
|---|---|---|---|---|---|
| Blank | –0.457 | 1897 | –121 | 82 | — |
| **PTZ** | | | | | |
| 0.04 | –0.446 | 364 | –139 | 83 | 80.8 |
| 0.2 | –0.424 | 130 | –189 | 96 | 93.1 |
| 1 | –0.508 | 95 | –108 | 126 | 95.0 |
| 5 | –0.505 | 55 | –114 | 112 | 97.1 |

### *3.3. Adsorption isotherm model research*

In order to study the adsorption information of PTZ adsorption on the Q235 steel surface. We used numerous adsorption isotherm models to explore the adsorption mechanism via EIS data. The fitted linear regression coefficients indicate that the adsorption of PTZ on the surface of Q235 steel conforms to the Langmuir adsorption isotherm model. The fitted data is listed in Figure 5. The Langmuir adsorption isotherm is as follow [30-33]:

$$\frac{C}{\theta} = \frac{1}{K_{ads}} + C \qquad (6)$$

where $C$ is the concentration of PTZ. $\eta$ indicates the surface coverage. $K_{ads}$ is the adsorption equilibrium constant. In order to explore the type of adsorption of PTZ on the Q235 steel surface. We used the following formula to calculate the $\Delta G^0_{ads}$ [34]:

$$K_{ads} = \frac{1}{55.5}\exp(-\frac{\Delta G^0_{ads}}{RT}) \qquad (7)$$

The fitted results are listed in Figure 5. The value of $K_{ads}$ is 97181.1 L/mol, and it is generally believed that a large $K_{ads}$ value indicates that PTZ can produce a close adsorption on the Q235 steel surface. In addition, the $\Delta G^0_{ads}$ value is –38.4 kJ/mol. Negative $\Delta G^0_{ads}$ value manifests that the adsorption of PTZ on the surface of Q235 steel is autonomous. Besides, when the $\Delta G^0_{ads}$ value is greater than –20 kJ/mol, it manifests that the adsorption of corrosion inhibitor on the surface of metal belongs to physical adsorption. When the value of $\Delta G^0_{ads} \leq$ –40 kJ/mol, the adsorption of corrosion inhibitor on the metal surface is chemical adsorption. When the value of –20 kJ/mol $\leq \Delta G^0_{ads} \leq$ –40 kJ/mol, the adsorption of corrosion inhibitor on the surface of metal belongs to the interaction of physicochemical adsorption [35-37]. Therefore, the PTZ adsorption on the surface of Q235 steel belongs to the interaction of physicochemical adsorption.

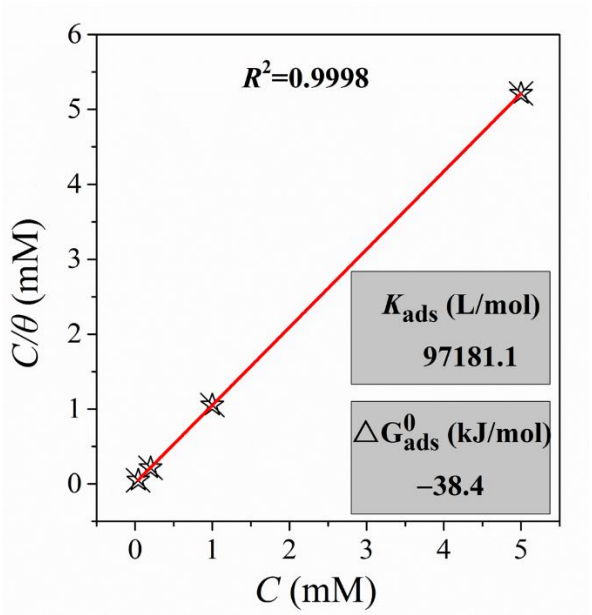


**Figure 5.** Fitted results of Langmuir isothermal adsorption.

*3.5. SEM analysis*

Figure 6 shows the surface morphology of Q235 steel under different conditions. Figure 6 (a) is the surface topography of Q235 steel immersed in 1 M hydrochloric acid with 5 mM of PTZ for 6 hours at 298 K. It can be found that the entire Q235 steel surface is relatively flat. Figure 6 (b) is the surface topography of Q235 steel immersed in 1 M hydrochloric acid for 6 hours at 298 K without PTZ. It can be found that the entire Q235 steel has been severely corroded. Corrosion holes are very obvious. An obvious corrosion pit appeared on the surface of Q235 steel. By comparing Figure 7(a) and (b), it can be shown that PTZ can exhibit excellent corrosion inhibition performance for Q235 steel in 1 M HCl. SEM experimental results and electrochemical data are highly consistent.

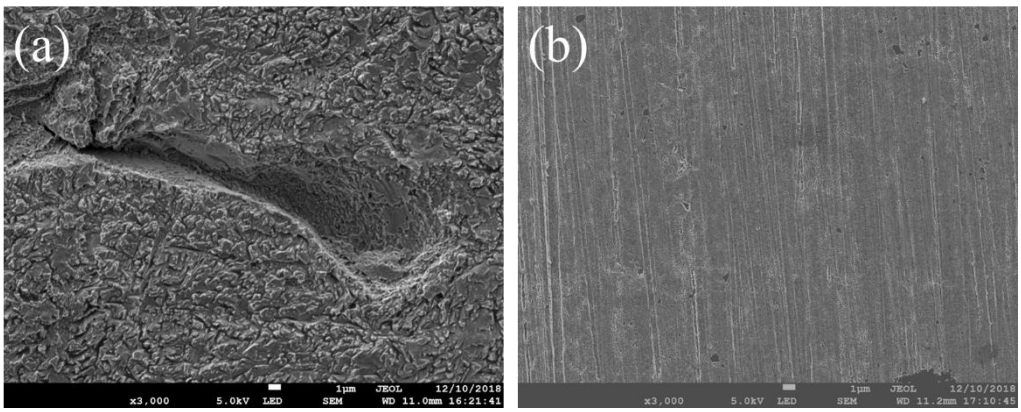


**Figure 6**. The surface morphology of Q235 steel under different conditions: (a) Q235 steel surface without 5 mM PTZ soaked in 1 M hydrochloric acid for 6 hours at 298 K, (b) Q235 steel surface with 5 mM PTZ soaked in 1 M hydrochloric acid for 6 hours at 298 K.

### *3.6. Quantum chemical calculation analysis*

Quantum chemical calculation is an effective way to predict the corrosion inhibition of corrosion inhibitor molecules. It can effectively predict the corrosion inhibition performance of the corrosion inhibitor by the nature of the corrosion inhibitor molecule, thereby saving a lot of material and financial resources. In this work, we calculated the frontier molecular orbitals, dipole moments, and electrostatic potential maps of PTZ molecule. The result of the calculation is presented in Figure 7.

In Figure 7, it can be found that the electrostatic potential map of PTZ consists of a red region and a blue region. The red region distributes on the five-membered ring containing four nitrogen atoms and the sulphur atom. While, the blue area is mainly distributed benzene ring. The red color of the ESP map has a nucleophilic nature, and the blue regions are electrophilic nature [38]. Therefore, it can be proved that PTZ participates in chemical bonding with Q235 steel mainly through nitrogen and sulphur -containing heteroatoms.

Frontier molecular orbital theory is widely used to study the electron cloud density distribution of corrosion inhibitor molecules. The electron cloud density of PTZ molecule distributed on the whole molecule. This shows that PTZ can be adsorbed on the surface of Q235 steel in parallel. The energy gap value ($\Delta E = E_{LUMO} - E_{HOMO}$) of PTZ is 3.98 eV. According to the references, usually a small gap value indicates that the corrosion inhibitor molecule has high corrosion inhibition performance [39-41]. From the energy gap, it can be judged that PTZ can show excellent corrosion inhibition performance.

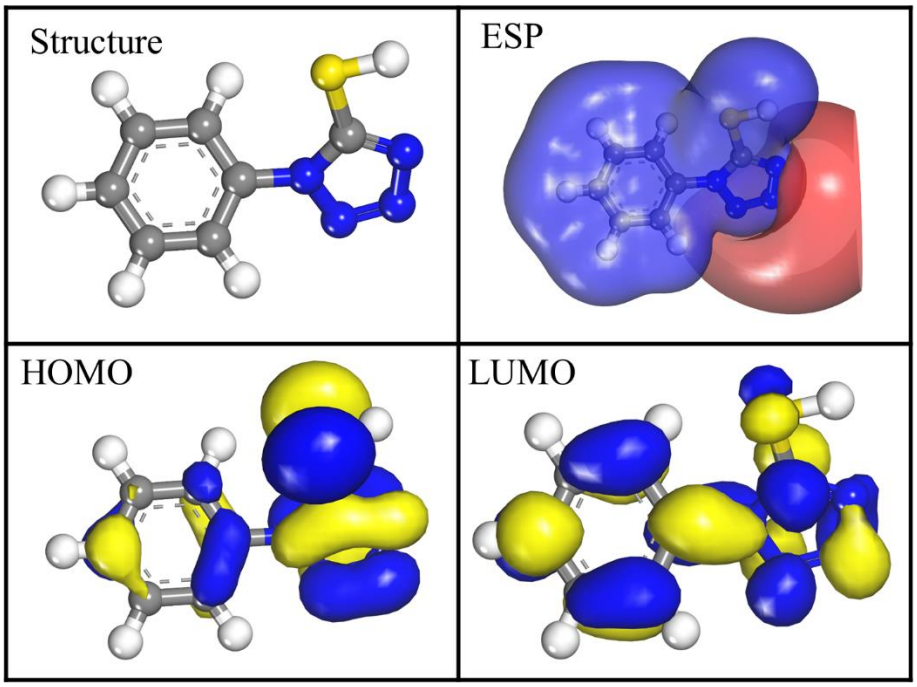


**Figure 7.** Results of quantum chemical calculations including PTZ-optimized configuration, electrostatic potential map, and electron cloud distribution of frontier molecular orbitals, respectively.

The dipole moment of PTZ is 5.48 Debye. Most corrosion workers believe that small energy gap values and large dipole moments correspond to superior corrosion inhibition performance. We can see

that PTZ has a small gap value and a large dipole moment. Therefore, it can be judged that PTZ molecules can show excellent corrosion inhibition performance. This is consistent with the experimental results.

*3.7 Molecular dynamics simulation*

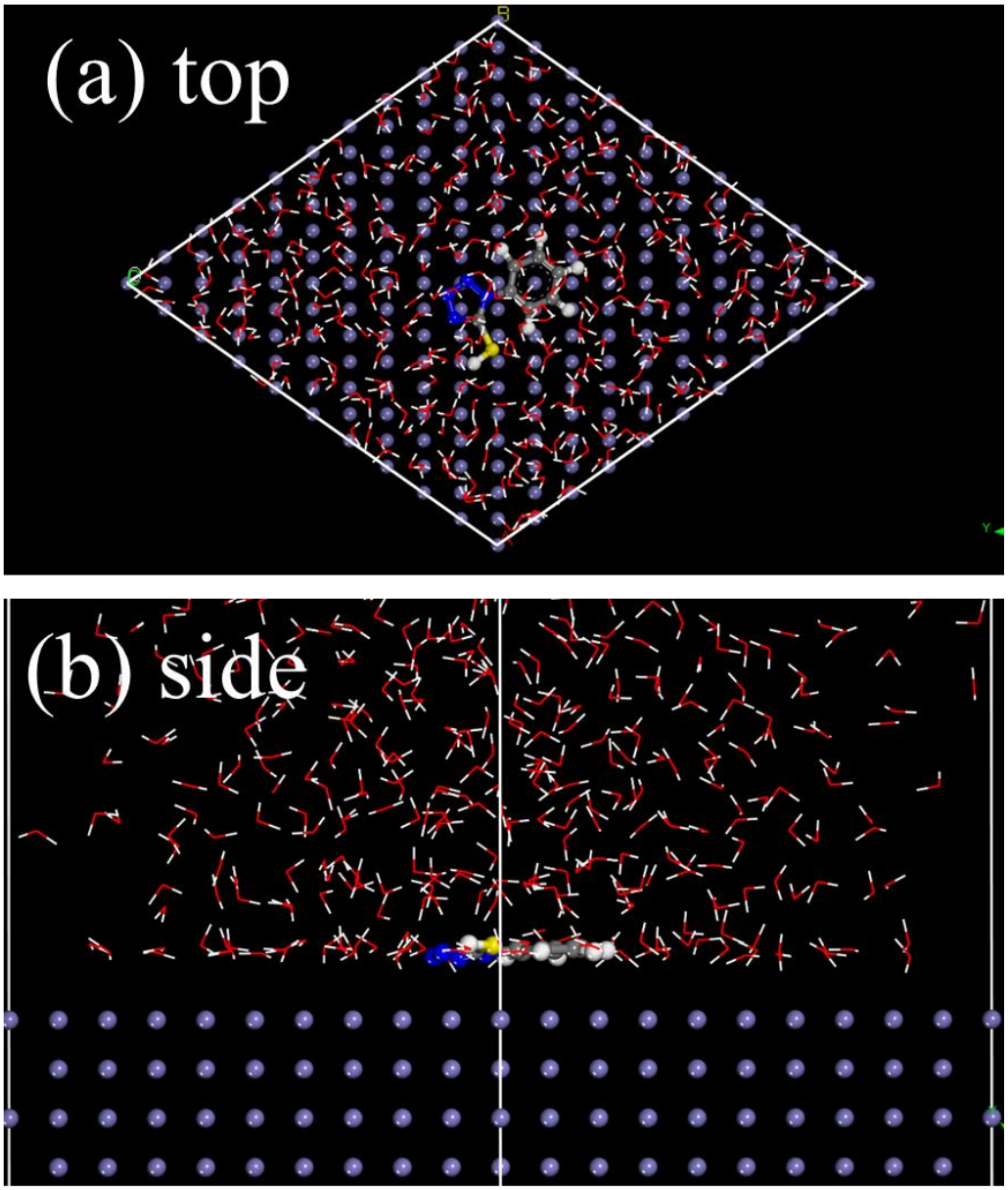


**Figure 8.** The (a) top and (b) side views showing the PTZ adsorption on the Fe (110) surface, respectively.

Molecular dynamics simulation (MDS) can effectively calculate the adsorption behavior of corrosion inhibitor molecules on metal surface. Figure 8 presents the stable adsorption configuration of PTZ molecule on the Fe (110) surface. It can be found that the PTE molecule adsorbs almost parallel on the Fe (110) surface via the nitrogen-containing five-membered ring and the S-hetero atom. This is

consistent with the results of previous quantum chemical predictions. In addition, we obtained the binding energy of PTZ molecules on the surface of Q235 steel by the following formulas [42, 43]:

$$E_{binding} = -E_{\text{int}\,eract} \quad (7)$$

$$E_{\text{int}\,eract} = E_{tot} - (E_{subs} + E_{inh}) \quad (8)$$

where $E_{binding}$ is the binding energy of PTZ adsorption on Q235 steel surface, $E_{tot}$ represents the total energy of the entire simulation system, $E_{subs}$ represents the total energy of the Fe(110) and $H_2O$, and $E_{inh}$ is the energy of the PTZ molecule. The binding energies of PTZ on the surface of Q235 steel is 455.6 kJ/mol. This indicates that the PTZ molecule has a strong adsorption capacity on the surface of Q235 steel, thus exhibiting excellent corrosion inhibition performance.

## 4. CONCLUSION

PTZ exhibits excellent anti-corrosion nature of Q235 in 1 M HCl. Electrochemical experiments data show that PTZ can restrain the cathodic and anodic reaction of Q235 steel, which is a mixed-type corrosion inhibitor. SEM morphology analysis strongly and vividly support the results of electrochemical tests. The adsorption of PTZ on the Q235 steel surface is consistent with Langmuir adsorption. Its adsorption type is a combination of physicochemical adsorption. Quantum chemical calculations strongly explore the active adsorption sites of PTZ molecule. Molecular dynamics simulations show that PTZ adsorbs on the Fe (110) surface in parallel model to obtain the largest coverage area.

ACKNOWLEDGMENTS
This work was supported financially by Project supported by the sponsored research program of chongqing university of science and technology for youth (ckrc2019046),the National Natural Science Foundation of China (51604052) and Natural Science Foundation of Chongqing, China (cstc2019jcyj-msxmX0064).

## References

1. Y. Yang, Y. Li, L. Wang, H. Liu, D. Lu, and L. Peng, *Int. J. Electrochem. Sci.*,14 (2019) 3375.
2. S. Y. Al-Nami, *Int. J. Electrochem. Sci.*,14 (2019) 3986.
3. P. Kannan, T.S. Rao, and N. Rajendran, *J. Colloid Interf. Sci.*, 512 (2018) 618.
4. Charitha B P, and Padmalatha Rao, *J. Ind. Eng. Chem.*, 58 (2018) 357.
5. N.D. Nam, P.V. Hien, N.T. Hoai, and V.T.H. Thu, *J. Taiwan Inst. Chem. E.*, 91 (2018) 556.
6. Ž.Z. Tasić, M.B. Petrović Mihajlović, M.B. Radovanović, A.T. Simonović, and M.M. Antonijević, *J. Mol. Struct.*, 1159 (2018) 46.
7. B. Tan, S. Zhang, Y. Qiang, W. Li, H. Liu, C. Xu, and S. Chen, *J. Mol. Liq.*, 286 (2019) 110891.
8. Y.J. Yang, H. Liu, D.M. Lu, L. Peng, and L. Wang, *Int. J. Electrochem. Sci.*, 14 (2019) 5008.
9. S. Xu, W. Li, X. Zuo, D. Zheng, X. Zheng, and S. Zhang, *Int. J. Electrochem. Sci.*,14 (2019) 5777.
10. H. M. Elabbasy, *Int. J. Electrochem. Sci.*,14 (2019) 5355.
11. M.R. Zahra Sanaei, Ghasem Bahlakeh, and Bahram Ramezanzadeh, *J. Ind. Eng. Chem.*, 69 (2019) 18.
12. R.N. Leili Rassoulia, and Mohammad Mahdavain, *J. Ind. Eng. Chem.*, 66 (2018) 221.
13. Ž.Z. Tasić, M.B. Petrović Mihajlović, M.B. Radovanović, and M.M. Antonijević, *J. Mol. Liq.*, 265 (2018) 687.
14. X. Zhang, and B. Tan, *Int. J. Electrochem. Sci.*, 13 (2018) 11388.

15. J. Du, Y. Liu, P. Liu, Y. Liu, S. Gao, and L. Zhang, *Int. J. Electrochem. Sci.*,14 (2019) 4532.
16. M. Ramezanzadeh, Z. Sanaei, G. Bahlakeh, and B. Ramezanzadeh, *J. Mol. Liq.*, 256 (2018) 67.
17. F. El-Hajjaji, M. Messali, A. Aljuhani, M.R. Aouad, B. Hammouti, M.E. Belghiti, D.S. Chauhan, and M.A. Quraishi, *J. Mol. Liq.*, 249 (2018) 997.
18. A. Biswas, P. Mourya, D. Mondal, S. Pal, and G. Udayabhanu, *J. Mol. Liq.*, 251 (2018) 470.
19. P.E. Alvarez, M.V. Fiori-Bimbi, A. Neske, S.A. Brandán, and C.A. Gervasi, *J. Ind. Eng. Chem.*, 58 (2018) 92.
20. M.M. Solomon, S.A. Umoren, M.A. Quraishi, and M. Salman, *J. Colloid Interf. Sci.*, 551 (2019) 47.
21. F. El-Hajjaji, M. Messali, M.V. Martinez de Yuso, E. Rodriguez-Castellon, S. Almutairi, T.J. Bandosz, and M. Algarra, *J. Colloid Interf. Sci.*, 541 (2019) 418.
22. M.B. Radovanović, and M.M. Antonijević, *J. Adhe. Sci. Technol.*, 31 (2016) 369.
23. J. Zhao, J. Zhang, J. Xie, H. Yang, W. Song, Y. Li, M. Zhao, X. Yang, *Int. J. Electrochem. Sci.*,14 (2019) 5472.
24. M. Corrales-Luna, M.T. Le, and E.M. Arce-Estrada, *Int. J. Electrochem. Sci.*,14 (2019) 4420.
25. N.K. Othman, S. Yahya, and M.C. Ismail, *J. Ind. Eng. Chem.*, 70 (2019) 299.
26. B.R. M. Motamedi, and M. Mahdavian, *J. Ind. Eng. Chem.*, 66 (2018) 116.
27. A. Mishra, C. Verma, H. Lgaz, V. Srivastava, M.A. Quraishi, and E.E. Ebenso, *J. Mol. Liq.*, 251 (2018) 317.
28. M. Abd El-Raouf, E.A. Khamis, M.T.H. Abou Kana, and N.A. Negm, *J. Mol. Liq.*, 255 (2018) 341.
29. L.L. Liao, S. Mo, H.Q. Luo, and N.B. Li, *J. Colloid Interf. Sci.* 520 (2018) 41.
30. Z.Z. Tasic, M.M. Antonijevic, M.B. Petrovic Mihajlovic, and M.B. Radovanovic, *J. Mol. Liq.*, 219 (2016) 463.
31. E. A. Flores-Frias, V. Barba , M.A. Lucio-Garcia, R. Lopez-Cecenes, J. Porcayo-Calderon, and J.G. Gonzalez-Rodriguez, *Int. J. Electrochem. Sci.*, 14 (2019) 5026.
32. X. Li, S. Deng, T. Lin, X. Xie, and G. Du, *J. Taiwan Inst. Chem. E.*, 86 (2018) 252.
33. E. Alibakhshi, M. Ramezanzadeh, G. Bahlakeh, B. Ramezanzadeh, M. Mahdavian, and M. Motamedi, *J. Mol. Liq.*, 255 (2018) 185.
34. M.B. Petrović Mihajlović, M.B. Radovanović, Ž.Z. Tasić, and M.M. Antonijević, *J. Mol. Liq.*, 225 (2017) 127.
35. B. Tan, S. Zhang, H. Liu, Y. Qiang, W. Li, L. Guo, and S. Chen, *J. Taiwan Inst. Chem. E.*, 102 (2019) 424.
36. K. Zhang, W. Yang, B. Xu, Y. Chen, X. Yin, Y. Liu, and H. Zuo, *J. Colloid Interf. Sci.*, 517 (2018) 52.
37. P. Han, C. Chen, W. Li, H. Yu, Y. Xu, L. Ma, and Y. Zheng, *J. Colloid Interf. Sci.*, 516 (2018) 398.
38. B. Tan, S. Zhang, H. Liu, Y. Guo, Y. Qiang, W. Li, L. Guo, C. Xu, and S. Chen, *J. Colloid Interf. Sci.*, 538 (2019) 519.
39. B. Tan, S. Zhang, Y. Qiang, L. Guo, L. Feng, C. Liao, Y. Xu, and S. Chen, *J. Colloid Interf. Sci.*, 526 (2018) 268.
40. B. Tan, S. Zhang, Y. Qiang, L. Feng, C. Liao, Y. Xu, and S. Chen, *J. Mol. Liq.*, 248 (2017) 902.
41. J. Zhang, L. Zhang, and G. Tao, *J. Mol. Liq.*, 272 (2018) 369.
42. B. Tan, S. Zhang, W. Li, X. Zuo, Y. Qiang, L. Xu, J. Hao, and S. Chen, *J. Ind. Eng.Chem.*, 77 (2019) 449.
43. A. Singh, K.R. Ansari, J. Haque, P. Dohare, H. Lgaz, R. Salghi, and M.A. Quraishi, *J. Taiwan Inst. Chem. E.*, 82 (2018) 233.